A fully coupled diffusion-reaction scheme for moisture sorption–desorption in an anhydride-cured epoxy resin

Jalal El Yagoubi [a,*], Gilles Lubineau [a], Frederic Roger [a], Jacques Verdu [b]

[a] King Abdullah University of Science and Technology (KAUST), Physical Science and Engineering Division, COHMAS Laboratory, Thuwal 23955-6900, Saudi Arabia
[b] Arts et Metiers ParisTech, Laboratoire PIMM, 151 Boulevard de l'Hopital, 75013 Paris, France

A B S T R A C T

Thermoset materials frequently display non-classical moisture sorption behaviors. In this paper, we investigated this issue from an experimental point of view as well as in terms of modeling the water transport. We used the gravimetric technique to monitor water uptake by epoxy samples, with several thicknesses exposed to different levels of humidity during absorption and desorption tests. Our results revealed that the polymer displays a two-stage behavior with a residual amount of water that is desorbed progressively. We proposed a phenomenological reaction-diffusion scheme to describe this behavior. The model describes water transport as a competition between diffusion and the reaction, during which the local diffusivity and solubility depend on the local advancement of the reaction. We then implemented our model using COMSOL Multiphysics and identified it using a MATLAB-COMSOL optimization tool and the experimental data. We discussed the relation between the hydrophilicity of the product of the reaction and the diffusion behavior. We examined the reaction-induced modification of the water concentration field. It is worth noting that part of the phenomenology can be explained by the presence of hydrolyzable groups.

Keywords:
Epoxy
Water transport
Diffusion-reaction

1. Introduction

In aeronautical and aerospace engineering, most currently used composites rely on epoxy-based thermoset materials because of their excellent mechanical properties that remain relatively stable even under warm temperature conditions. Yet, during flight, these composites are commonly exposed to both thermomechanical cycling and high humidity. One consequence of these severe environmental conditions is the progressive modification over time of the epoxy's behavior. To be properly designed, these epoxy resins require full characterization under environmental conditions. We focus on water sorption behaviors in short-term aging of epoxies in this paper.

Water uptake has a detrimental effect on the mechanical properties of polymers. First, water is known to act as a plasticizer for such materials. A decrease in the glass transition temperature (T_g) is observed [1–4], reducing the maximum operating temperature. De Neve et al. [2] reported a decrease in the glass transition temperature of 25 °C with a 3% mass uptake, as well as a drop in the glassy (3.4 GPa–2.2 GPa) and rubbery modulus (70 MPa–25 MPa) as a function of the mass uptake. In a different epoxy system, Alessi et al. [5] showed a decrease of the fracture toughness (0.8 MPa $m^{0.5}$–0.5 MPa $m^{0.5}$) after immersion for one week in distilled water at 70 °C. In addition, the ingression of water leads to an increase in the volume of the polymer [1,4,6–10]. Commonly, the global hydric strain, derived from the volume increase, is linked to the mass uptake by a macroscopic coefficient of moisture expansion. Hence, water uptake modifies both the stress/strain distribution inside the structure and the local mechanical properties of the constitutive material. Moreover, in many cases (heterogeneous materials, complex structural shapes, cyclic conditions) the concentration of water is not homogeneous. Understanding of the gradient of water absorption and the consequential material modification is needed to predict micromechanical damage.

A convenient way to investigate absorption kinetics from a macroscopic point of view is to monitor the mass uptake that accounts for the overall amount of water molecules absorbed by the material using gravimetric analysis. These tests lead to a useful overall understanding of water sorption. Gravimetric curves can reveal Fickian behaviors or complex features (frequently called anomalies [11]) that suggest that there are complex underlying mechanisms.

Many experimental works have reported non-classical sorption behaviors. A typical non-classical behavior frequently encountered

* Corresponding author. Tel.: +966 (0)565 560 239.
E-mail address: jalal.yagoubi@kaust.edu.sa (J. El Yagoubi).

involves two-stage with (1) an initial linear increase with respect to the square root of time (according to Fick's model) and (2) a deviation from Fick's model without stabilization of the mass uptake for the investigated time window [4,6,9,10,12–18]. A number of authors proposed several explanations for these observations, some of which are mentioned below. The first family of models is based on the assumption of non-constant parameters in the classical Fickian model. These include the diffusion parameter that governs the diffusion rate and the concentration at the boundary.

- Based on experimental measurements in [19,20] proposed a model with a concentration-dependent diffusion parameter that is reduced under high relative humidity.
- The anomalies of the sorption behaviors reported by [7,13,21] were interpreted under the framework of molecular relaxation theory. A time-dependent diffusion parameter was used to reproduce the experimental observations.
- The model proposed by Weitsman [22] is often used to describe the two-stage sorption behavior of viscoelastic materials. The retardation process due to viscoelasticity was taken in consideration in this model using time-dependent boundary conditions.

These approaches are suitable and used to fit absorption curves but fail in reproducing some of the experimental observations particularly during desorption. Therefore, another family of models considers the partition of water uptake into two species that are commonly called "bonded" and "unbounded" water molecules. There is currently no consensus on the definition of these terms:

- In the Carter and Kibler model (Langmuir-type model) [23], "bonded" water refers to the molecules that create low energy bonds with hydrophilic sites while "unbounded" water refers to water transported in free volume. In Ref. [24] the suggestion is made that a physical interpretation be offered in the light of NMR analysis performed on wet samples.
- In Ref. [17], the deviation from the Fickian model is attributed to microcavities developed during absorption. It is assumed that the "bonded" water is a combination of both the "bonded" and free water following the classical Langmuir description. Free water is the water that resides in the voids that are created.
- The incomplete cure of the epoxy is also used as a justification for non-Fickian behavior [4,9,15]. A reasonable explanation is given by [15]. It focuses on the hydrolysis of the residual epoxy groups. The "bonded" water would correspond to the part of sorbed water that has reacted with the epoxy.

It is worth noting that in common in these three models is that they are based on a diffusion-reaction scheme. Nevertheless, the models differ in some aspects that can be highlighted when a desorption test is performed.

In this paper, we propose a phenomenological reaction-diffusion scheme. Local material parameters depend on the local advancement of both the diffusion and the reaction mechanisms. This model unifies and extends the approaches mentioned to create a framework that can reproduce both sorption and desorption behaviors on samples of various thicknesses. An experimental validation of the approach is proposed and a initial insight about the identification strategy used in this model is offered.

In the remainder of this paper, we first describe the commercial epoxy resin under study as well as the sample preparation method. Then, we investigate the sorption behavior of the resin using the gravimetric technique. We present our model formulation in the fourth section. Then, we present results from numerical simulations using COMSOL Multiphysics software and we identify the parameters using an original identification strategy in MATLAB-COMSOL. Finally, we discuss the reaction-induced modification of the diffusion behavior and the consequences on the water concentration field.

2. Materials and methods

A commercially available epoxy system with a high glass transition temperature (EPOLAM 2063 supplied by Axson Technologies) was the focus of our study in this research. As its viscosity at 75 °C is very low, this resin is used in the manufacturing of composites using transfer molding or infusion techniques. It is a two-component epoxy resin based on a mixture of several epoxy monomers. It is mainly a blend of cycloaliphatic epoxy resin and a diglycidyl ether of bisphenol-A (DGEBA) resin. The resin was mixed at 75 °C with an anhydride hardener, also provided by Axson Technologies, with a volume ratio of 1:1 (100:107 mass ratio) that corresponds to the stoichiometry between the anhydride and the epoxy. The mixture was stirred for 15 min at the same temperature to obtain a homogeneous blend. Then, an adequate quantity of resin was poured into a flexible thermoplastic mold with a non-stick surface. Degassing was performed inside a vacuum chamber (Struers Citovac) at 0.1 bar. The epoxy preparation was completed following the two-step curing cycle recommended by the supplier and described hereafter. First, the blend was kept at 80 °C for 6 h and then cooled to the ambient temperature. After removal from the molds, the samples were heated to 180 °C and post-curing was completed after 4 h. The neat resin sheets were then maintained inside a desiccator at room temperature.

The glass transition temperature T_g of the resin was evaluated by a dynamic mechanical analysis (DMA) instrument (Netzch DMA 242 C) in the three-point bending mode at 1 Hz and 5 °C/min. The measured value (135 °C) was significantly lower than the maximum T_g given by the supplier (190 °C). Incomplete curing of the epoxy was confirmed by DMA performed at various post-curing times. Table 1 shows that the T_g increased as the post-curing time increased. It is clear that the retained curing cycle used in this experiment did not fully cure the epoxy, and the conversion was less than 1. Below, part of the phenomenology is explained by the presence of residual epoxy and anhydride that did not react and this observation becomes important there. Finally, three specimen thicknesses were considered: $2L = 1$ mm, $2L = 435$ μm and $2L = 250$ μm. To meet equipment specifications, 10 mm by 15 mm samples were obtained by cutting the raw plates using a diamond saw. The thickness of each specimen was adjusted by grinding the surfaces with SiC abrasive paper (# 1000) (scattering of the thickness was about 4 μm).

3. Experimental results

The gravimetric analysis was conducted on a IGASorp-HT system (Hiden Isochema). This instrument is a dedicated system that monitors mass uptake and sorption kinetics including

Table 1
Evolution of the glass transition temperature (T_g) of EPOLAM 2063 as a function of the post-curing time. The standard curing cycle is 6 h at 80 °C + 4 h at 180 °C.

Post-curing cycle	T_g (°C)
Standard	135
Standard + 2 h at 180 °C	160
Standard + 4 h at 180 °C	180
Standard + 6 h at 180 °C	180

a microbalance with 0.1 μg resolution and precise control of both temperature and humidity.

Samples were placed inside an isolated chamber on a stainless steel mesh sample holder that was 15 mm in diameter. The tests were conducted at a constant temperature (50 °C) and relative humidity (40%, 60% or 90%). The testing procedure was as follows. Prior to the start of the absorption analysis, samples were first dried until equilibrium was reached. Then, a stream of moist air was circulated at 250 mL/min in the chamber. The partial pressure of the water was controlled by mixing a dry nitrogen flow with a wet air flow. It is worth noting that an interesting aspect of the technique used here was that we avoided experimental errors introduced when samples were taken out from the chamber for weighting. Also, this technique has the advantage of allowing the mass sample, $m(t)$, to be collected at a rather high rate (every 3–8 min).

The overall mass uptake, $m_w^{\exp}$ (Eq. (1)), is defined as the ratio of the mass of water absorbed by the resin, Δm (Eq. (2)), to the mass of the initial sample at the dried state, m_0.

$$m_w^{\exp} = \frac{\Delta m(t)}{m_0} \tag{1}$$

where:

$$\Delta m(t) = m(t) - m_0 \tag{2}$$

Several samples were tested, but for clarity, results from only one test are reported since the experiment appears to be reproducible with a negligible deviation. The evolution of the mass uptake (m_w) in relation to time is plotted for all experimental configurations (% RH, sample thickness) in Figs. 1 and 2. In Fig. 3, the mass uptake, for the tests performed at 60%RH on the three thicknesses, is plotted versus $\sqrt{t}$ (Fig. 3(a)) and versus $\sqrt{t}/2L$ (Fig. 3(b)). Before we present a detailed description of the phenomena involved in the water absorption, we give some general observations. First, the mass uptake did not stabilize during the experimental time window. In addition, the general shape of the curves is characteristic of a two-stage behavior. Concerning the

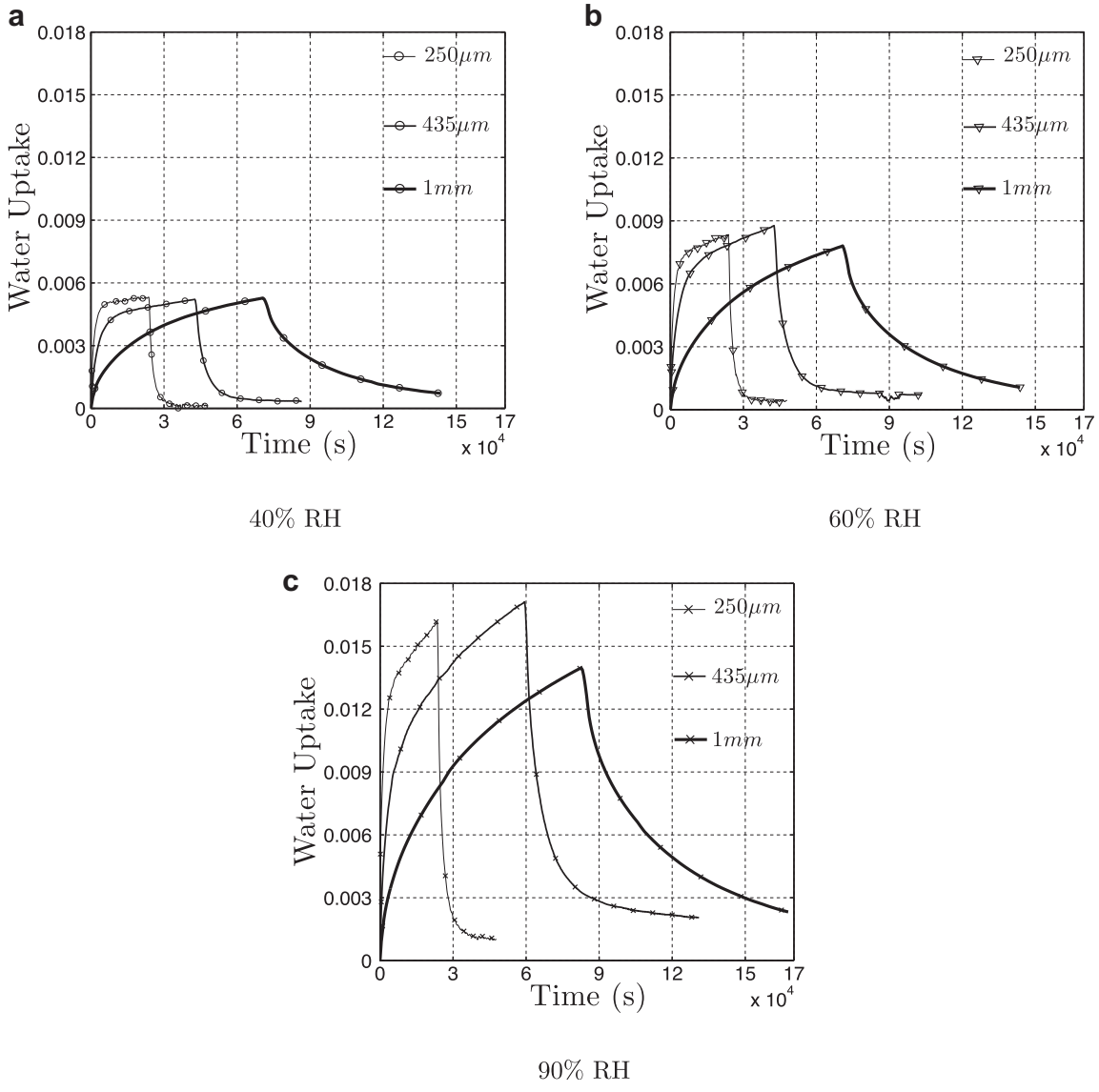

Fig. 1. Evolution of the mass uptake of the epoxy samples (EPOLAM 2063) with several thicknesses and exposed to different levels of humidity (at 50 °C) and effects of the sample thickness (1 mm, 435 μm and 250 μm).

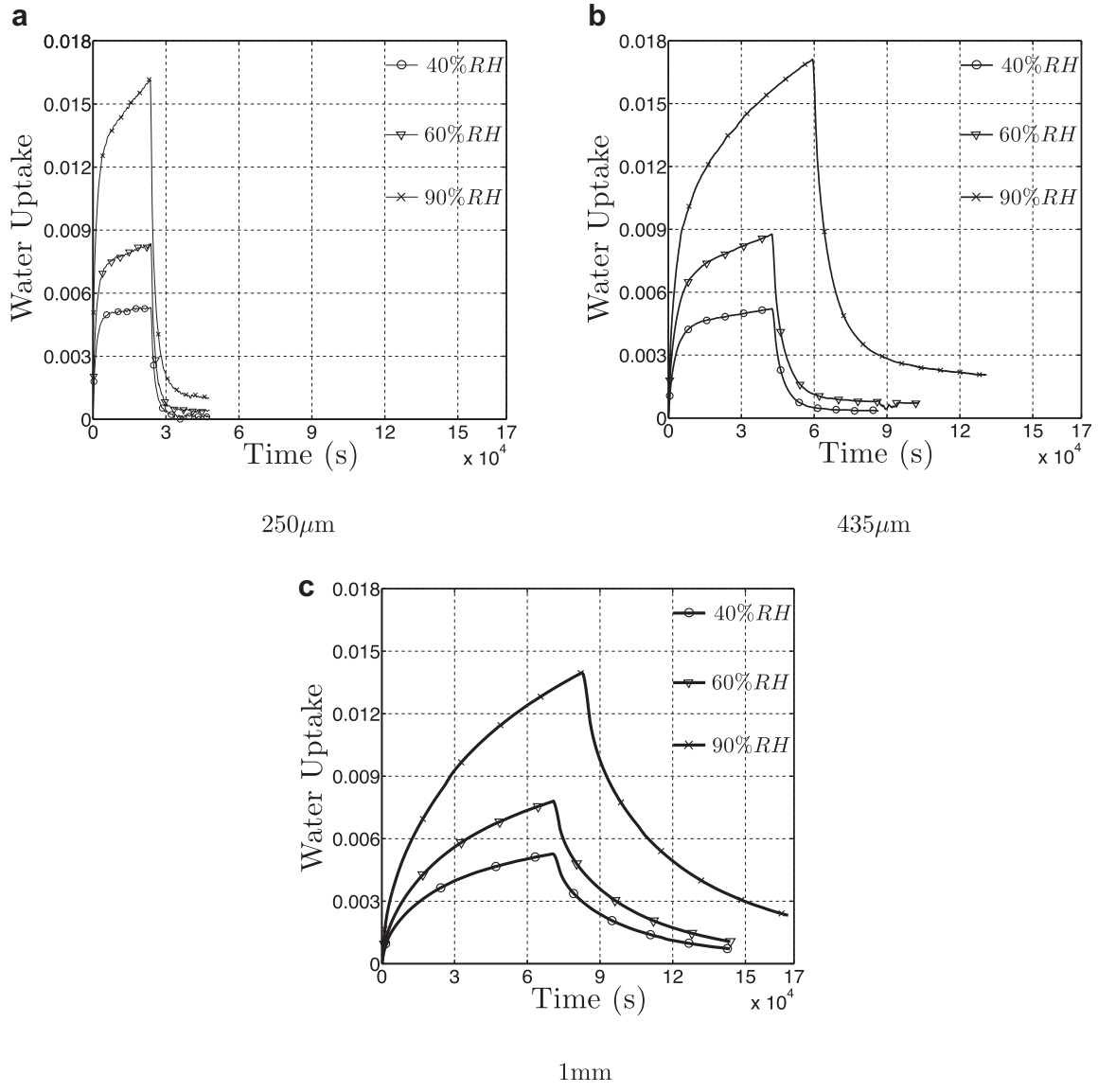

Fig. 2. Evolution of the mass uptake of the epoxy samples (EPOLAM 2063) with several thicknesses and exposed to different levels of humidity (at 50 °C) and effects of the environmental humidity content (40%, 60% and 90%).

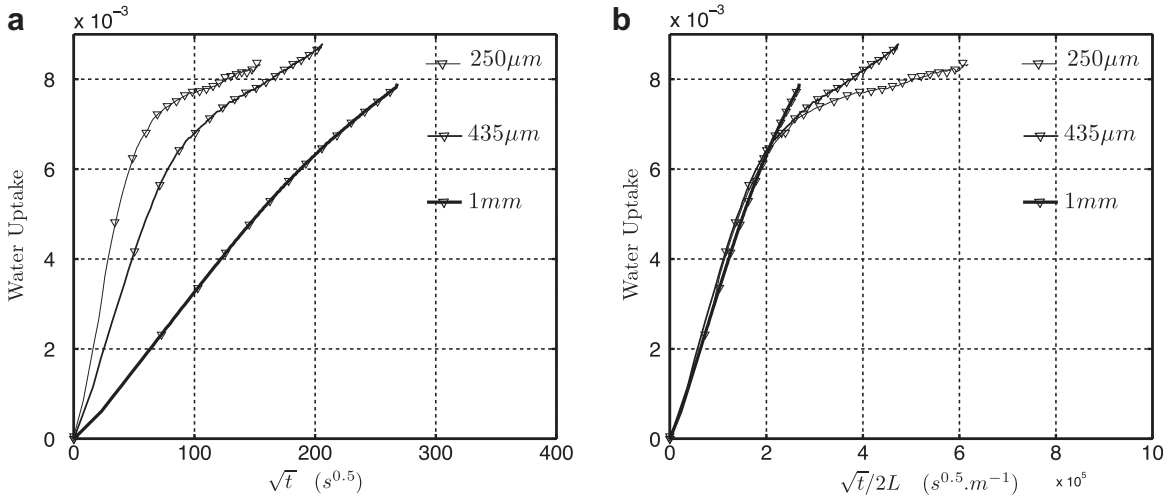

Fig. 3. Evolution of the mass uptake of the epoxy samples (EPOLAM 2063) with several thicknesses and exposed to 60%RH (at 50 °C) versus $\sqrt{t}$ and versus $\sqrt{t}/2L$ (film thickness scaling).

amount of water absorbed by the material, the low hydrophilicity of the material with a maximal mass uptake ranging from 0.5% (at 40% RH) to 1.6% (at 90%RH) is remarkable.

Nevertheless, the curves do display some basic features of Fickian behavior. At first, the mass uptake increases linearly with respect to the square root of time. Fig. 3(b) shows that the first linear portion of the absorption curves are superimposed when plotted as a function of $\sqrt{t}/2L$, confirming the film thickness scaling that is characteristic of a Fickian equation.

Then, we observe a transition to a second stage after a period of about 160 min. Fig. 3(b) indicates that the film thickness scaling is no more verified. The kinetics at this stage appears to be driven by a reactive process as it does not depend on the thickness but rather on the %RH. At a given %RH, the sorption kinetics is then almost independent of the thickness as illustrated on the common slope of all curves in Fig. 3(a).

Finally, after desorbing the material for a period equal to the absorption time, the mass evolution reveals the presence of a residual amount of water in the polymer. However, this residual mass is not permanent because the mass of the sample continues to decrease at the end of the experiment. Furthermore, it is worth noting that the desorption process is significantly slower than the absorption process.

4. Modeling water transport

In accordance with the experimental observations, we propose to adopt a general approach that consists of modeling water transport by assuming two basic mechanisms: diffusion and reaction. At any point in the domain Ω (Fig. 4), the following three species can coexist with corresponding concentrations (mol m^{-3}):

- *w*: water molecules that remain free to diffuse in the polymer network;
- *R*: the reactive substrate;
- *Y*: a complex formed by the reaction between the diffusing water molecules and the reactive substrate.

The formation/dissociation kinetics of the complex is described by a global reactive term that we call r_w.

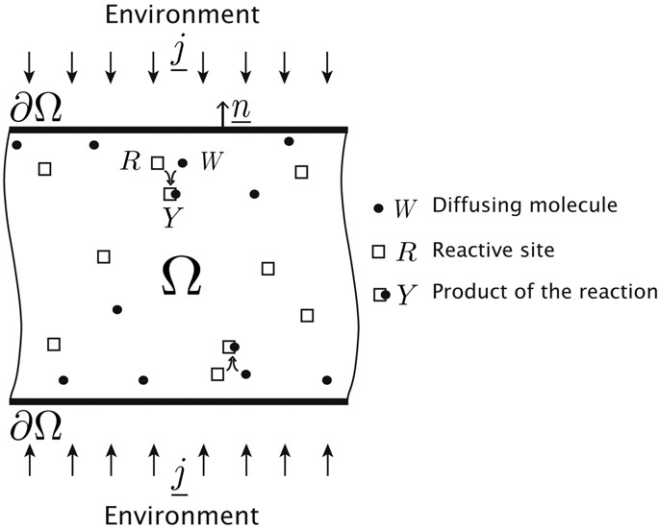

Fig. 4. Description of the diffusion-reaction problem: three different species coexist in the domain Ω.

4.1. Conservation equation

The mass conservation of the water in a defined domain (Ω) exposed to a humid environment at the boundary (∂Ω) leads to Eq. (3).

$$\frac{\mathrm{d}}{\mathrm{d}t}\int_{\Omega} w \quad \mathrm{d}\Omega = \int_{\partial\Omega} -\underline{j}\cdot\underline{n} \quad \mathrm{d}\partial\Omega + \int_{\Omega} r_w \quad \mathrm{d}\Omega \tag{3}$$

where $\underline{j}$ is the mass flux of the water molecules and $\underline{n}$ is the outward normal.

Neglecting the volume variation due to moisture absorption, Eq. (3) leads to the following local equation:

$$\frac{\partial w}{\partial t} = -div(\underline{j}) + r_w \tag{4}$$

Then, we need to define the mass flux, $\underline{j}$, and the kinetics of the reaction term, r_w.

4.2. Modeling of the diffusion process

The mass flux is derived from the chemical potential of the diffusing species, *w*, as follows (Eq. (5)):

$$\underline{j} = -Mw\,\underline{\nabla}\,\mu^w(a,T) \tag{5}$$

where *M* and μ^w are, respectively, the mobility and the chemical potential. Classically, the following expression holds for μ^w (Eq. (6)):

$$\mu^w(a,T) = \mu_0^w + RT\ln(a) \tag{6}$$

in which *a* is the activity, *R* the universal gas constant (8.314 J/K mol) and *T* the temperature (K). Assuming low concentrations, which is consistent with the observed material's hydrophilicity, the activity can be approximated by (Eq. (7)):

$$a = \frac{w}{w_s} \tag{7}$$

where w_s is the local maximum concentration that the material can absorb.

Then, (Eq. (8)):

$$\mu(w,T) = \mu_0 + RT\ln\left(\frac{w}{w_s}\right) \tag{8}$$

The maximum reachable water concentration, w_s, is assumed to follow Henry's law (Eq. (9)):

$$w_s = Sp_w \tag{9}$$

where *S* is the local solubility of water in the polymer network (mol m^{-3} Pa^{-1}) and p_w is the partial pressure of water in the environment (Pa). The partial pressure (Eq. (10)) can be written as a function of the water activity in the environment (a^e) and the saturation vapor pressure in air, p_{sat} (Pa) (for which we retain Rankin's approximation, Eq. (11)).

$$p_w = a^e p_{sat}(T) \tag{10}$$

$$p_{sat}(T) = 1.01325\text{x}10^5 \cdot e^{13.7-\frac{5120}{T}} \text{ (Rankin's saturation vapor pressure)} \tag{11}$$

In the case when the temperature is uniform throughout the material, the mass flux is given by Eq. (12):

$$\underline{j} = -MRT\left(\underline{\nabla} w - \frac{w}{w_s}\underline{\nabla} w_s\right) \tag{12}$$

Remark: It is worth noting that if the material (and thus the solubility) is also uniform, Eq. (12) can be reduced to Fick's well-known first law that involves the classical diffusion coefficient, D (m^2/s):

$$D = MRT \tag{13}$$

The original Fickian model describes water sorption as a diffusion mechanism at a constant rate and constant solubility.

In the case when there are simultaneous diffusion and reaction processes, the material is no longer spatially uniform and a gradient of properties exists. The evolution of the microstructure [17] or of the polymer network itself [15] has an impact on the diffusion process. From a macroscopic and phenomenological point of view, we propose to model this effect with a dependency of the local mobility and the local solubility to the advancement of the reaction.

Remark: It is important to note that, in our approach, the progress of the reaction can modify both the transient and the steady-state properties. A modification of the mobility would affect only the diffusion kinematics, and not the equilibrium state. An evolution of the solubility would modify the steady-state concentration.

A molecular approach could help to define D as a function of the size of the diffusing particles [25] and the polymer structure and microstructure. We consider here only a macroscopic approach for which the diffusion parameter follows an Arrhenius-type law:

$$D(T,Y) = \widehat{D}(Y)\cdot e^{\frac{-E_a^t(Y)}{RT}} \tag{14}$$

where E_a^t is the activation energy of the transport mechanism. As a first approximation, the pre-exponential factor $\widehat{D}$ does not depend on the temperature. Yet, it might depend on the local evolution of the microstructure or the polymer network that modifies the frictions experienced by the diffusing particles. We assume that the structural and the microstructural evolutions can be quantified by the concentration of the products of reaction Y. A simple linear relationship that corresponds to a linearization for a low level of transformation is retained:

$$\widehat{D}(Y) = \widehat{D_0} + \widehat{D_1}\cdot Y \tag{15}$$

$$E_a^t(Y) = E_{a0}^t + E_{a1}^t\cdot Y \tag{16}$$

Similar considerations of the solubility lead to the following equations (Eq. (17)). A linear approximation is adopted for the pre-exponential parameter, $\widehat{S}$ (Eq. (18)), and for the heat dissolution, H_s (Eq. (19)):

$$S(T,Y) = \widehat{S}(Y)\cdot e^{\frac{-H_S(Y)}{RT}} \tag{17}$$

$$\widehat{S}(Y) = \widehat{S_0} + \widehat{S_1}\cdot Y \tag{18}$$

$$H_s(Y) = H_{s0} + H_{s1}\cdot Y \tag{19}$$

4.3. Modeling the reaction process

As mentioned in the introduction, several models have been developed on the basis of a diffusion-reaction scheme. All of these models postulate that the absorbed water is in two states. They propose several rate laws to describe the transformation from one state to the other. Here, the absorbed water can either take the form of water molecules, w, or the form of a complex formed by the reaction (Y), which, in general, can be a cluster or a new chemical species.

The adopted formulation of the rate law is based on the kinetic model suggested by [15]. They considered the hydrolysis of the epoxy group. This approach was extended by [26] for a reversible reaction involving the three species (w, R and Y) (Eq. (20)) and a non-constant solubility to take into account the hydrophilicity of Y. In the case of a first-order chemical reaction occurring at a constant volume, the rate law is given by Eq. (21). It is a function of the concentrations of the reactants (w, R) and the products (Y) and of the two rate constants (k_h, k_r) that are supposed to be dependent only on temperature.

$$w + R \leftrightarrows Y \tag{20}$$

$$r_w = -k_h(T)wR + k_r(T)Y \tag{21}$$

This expression (Eq. (21)) is retained for two main reasons.

- First, the physical explanation evoked by [15] is consistent with our experimental results (Table 1) as the resin was not fully cured. Here, the curing process result in the presence of several groups that can be hydrolyzed. This can be a reasonable explanation for this specific sorption behavior and will be discussed below.
- Second, this relation is rather general and may be considered as an initial phenomenological law. In particular, it is equivalent to the one given by Carter and Kibler [23] if we assume a constant concentration of reactive sites, R, which is the case when the reactive substrate, R, is clearly in excess.

Finally, considering isothermal conditions ($T = 50\ ^\circ C$), the governing equations of the model are summarized as follows:

Conservation equations:

$$\frac{\partial w}{\partial t} = -div(\underline{j}) + r_w \tag{22}$$

$$\frac{\partial Y}{\partial t} = r_Y \tag{23}$$

$$\frac{\partial R}{\partial t} = r_R \tag{24}$$

Constitutive equations:
Diffusion law:

$$\underline{j} = -D(Y)\left(\underline{\nabla} w - \frac{w}{w_s(Y)}\underline{\nabla} w_s(Y)\right) \tag{25}$$

$$D(Y) = D_0 + D_1\cdot Y \tag{26}$$

$$w_s(Y) = (S_0 + S_1\cdot Y)a^e p_{sat} \tag{27}$$

Reaction kinetics:

$$r_w = -k_h(T)wR + k_r(T)Y \tag{28}$$

$$r_R = -k_h(T)wR + k_r(T)Y \tag{29}$$

$$r_Y = k_h(T)wR - k_r(T)Y \tag{30}$$

4.4. Boundary and initial conditions

At the interface between the polymer and the humid air, the chemical potential of water in both media is equal at equilibrium. Moreover, at the boundary of the domain ($\partial\Omega$), the water concentration, w, is assumed to follow Henry's law (Eq. (31)).

$$w = Sa^e p_{\text{sat}} \quad \forall \underline{M} \in \partial\Omega, \quad \forall t \tag{31}$$

The water activity in the environment (a^e) is set in accordance with the experimental conditions. From the initial time ($t = 0$) to the end of the absorption stage, it takes the values of 0.4, 0.6 or 0.9, and it is then set to zero until the end of the test (during the desorption stage).

The initial conditions are summarized in the Eq. (32). First, it is assumed that the material is dry before the start of the gravimetric experiments. Although [27] reported that the polymer can exhibit a two-phase microstructure with a crosslinking gradient, we assume as an approximation that the initial field of reactive sites is homogeneous, taking the value R_0 across the whole domain.

$$\begin{aligned} w &= 0 \quad \forall \underline{M} \in \Omega, \quad t = 0 \\ Y &= 0 \quad \forall \underline{M} \in \Omega, \quad t = 0 \\ R &= R_0 \quad \forall \underline{M} \in \Omega, \quad t = 0 \end{aligned} \tag{32}$$

Then, all quantities evolve both in time and space during the whole absorption/desorption process following the equations Eqs. (22)–(30).

5. Numerical implementation

5.1. Model implementation with COMSOL Multiphysics

We implemented the model introduced in the previous section using COMSOL Multiphysics 4.2 Software. It includes a Partial Differential Equation for the mass conservation equation (Eq. (22)) and two Ordinary Differential Equations for the reaction kinetics (Eq. (23) and Eq. (24)). We conducted one-dimensional (1D) simulations in this work with the geometry and boundary conditions given in the Fig. 5, assuming that the epoxy plate was infinite in its plane. The relevance of this assumption was confirmed by three-dimensional simulations showing that the relative difference in the maximum mass uptake is less than 3%. Considering the symmetry, only half of the thickness was modeled and meshed with one-dimensional quadratic elements. The thickness ($2L$) as well as the activity (a^e) are parameters that take different values ($2L = [1\text{ mm}, 0.435\text{ mm}, 0.250\text{ mm}]$, $a^e = [0.4, 0.6, 0.9]$). The global problem is solved with the MUMPS solver and the BDF scheme for the time discretization with a free time stepping.

For each experimental configuration (thickness, %RH), the evolution of the concentration fields (w, R and Y) were simulated. Then, neglecting the swelling of the material, we derived the mass ratio of the overall absorbed water from the average concentrations of Y and w in Ω according to the Eq. (33).

$$m_w^{num} = \frac{\Delta m}{m_0} = \frac{M_{\text{H}_2\text{O}} \int_\Omega w + Y \mathrm{d}V}{\rho_0 V_o} \tag{33}$$

where $\rho_0 = 1160\text{ kg m}^{-3}$ is the initial density of the polymer and $M_{\text{H}_2\text{O}} = 18 \times 10^{-3}$ kg/mol is the molar mass of water.

Hereafter, this global quantity is compared with the experimental data to identify the model parameters.

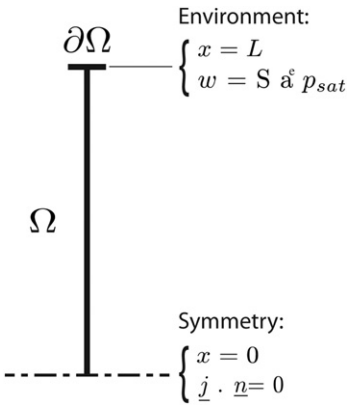

Fig. 5. Representation of the geometry and the boundary conditions considered for the numerical implementation.

5.2. Model identification using genetic algorithms

First, the diffusion process (mass flux) is characterized by four parameters. D_0 and S_0 are the initial Fickian parameters and D_1 and S_1 describe, respectively, the evolution of the diffusion parameter and the solubility as a function of the progress of the reaction (Eq. (26) and Eq. (27)). Then, the reaction kinetics is described by a set of three parameters: the two rate constants, k_h, k_r, and the initial concentration of the reactive sites, R_0.

The seven parameters are estimated using a suitable identification procedure, as described in Fig. 6. It consists of splitting the optimization into three iterative steps. In each step, we identify a set of parameters on different sections of the curves (hereafter called the time window) assuming that the other parameters are known from the previous iteration (fixed parameters).

- At the initialization step, we neglect the reaction ($Y = 0$) and only the two linear Fickian parameters, D_0 and S_0, are optimized for the time window [0: t_d], where t_d is selected based on the experimental data.
- The identified parameters (D_0, S_0) are then used as the input for the second step, in which the direct reaction is considered while the reverse reaction is omitted. The optimization parameters are R_0, k_h and S_1 identified on the time window [0: t_{abs}]. At the end of this step, if the comparison between the simulation and the experiments is satisfactory, we moves to the third step; otherwise, we return to the first step using the updated values for R_0, k_h and S_1.
- Finally, the third step is devoted to the estimation of the two remaining parameters, k_r and D_1, considering the whole experimental time window [0: $t_{\max}$]. Again, if the numerical results do not agree with the experimental data, we return to the second step using updated values for k_r and D_1; otherwise, the optimization process is completed.

At each of the mentioned steps, minimization is performed with an automated tool (OPTIM) using COMSOL and the MATLAB genetic algorithm functions.

Fig. 6 depicts the main steps of the genetic algorithm, including the communication between MATLAB and the COMSOL server. A genetic algorithm is an adaptive identification method able to generate individual solutions through reproduction techniques (Selection, Crossover and Mutation) in order to converge to the optimal one. Hence, for each generation, a score is affected to each individual by the fitness function that returns a vector (Multi-objective algorithm) with the errors related to the different

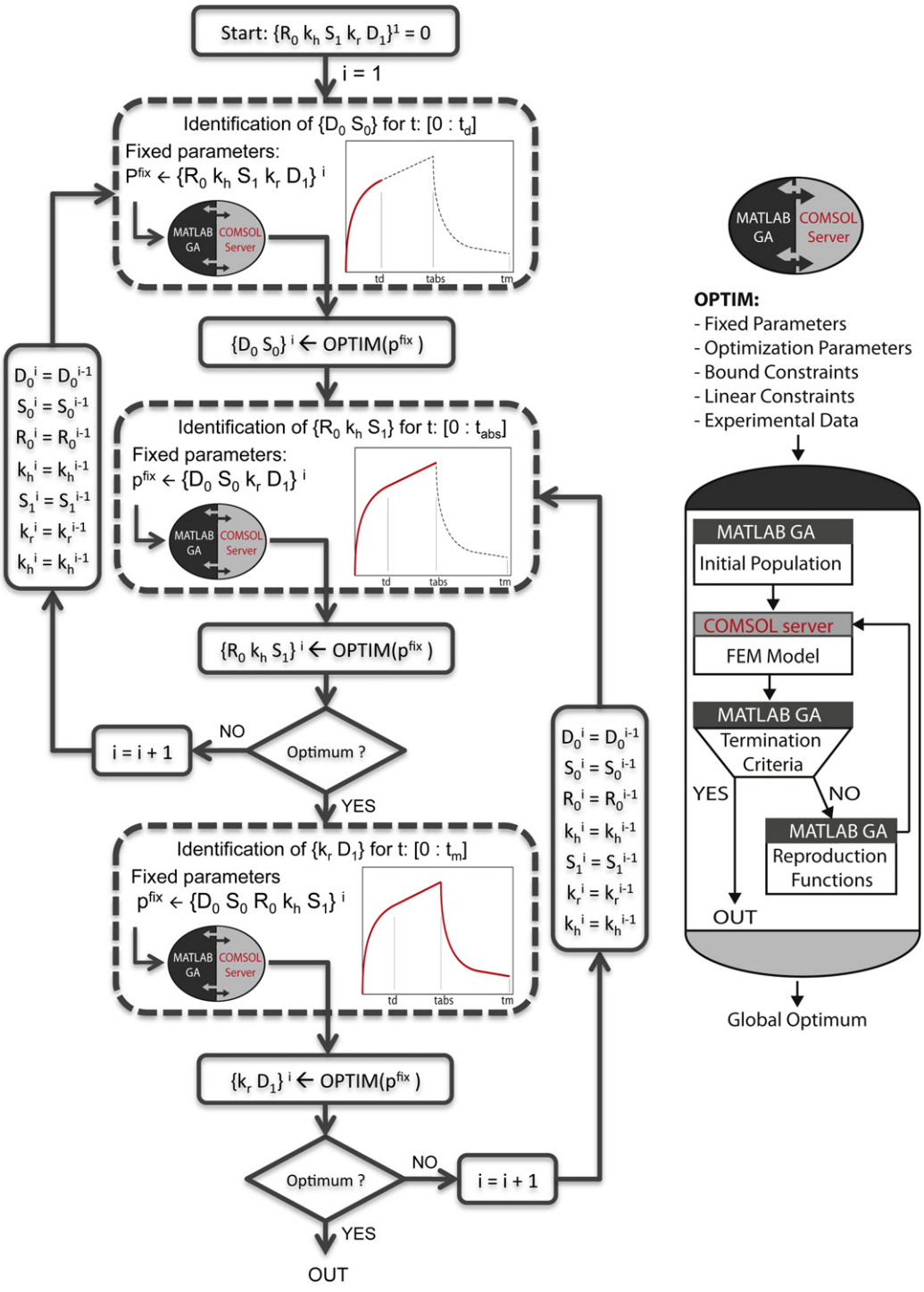

Fig. 6. Flowchart of the identification procedure using MATLAB and the COMSOL server.

experiments. The elementary errors, F_j, are the mean distance in the time window [0: t_L] between the calculated mass uptake (Eq. (33)) and the experimental data according to Eq. (34).

$$F_j(t_L) = \frac{1}{t_L}\int_{t=0}^{t=t_L} \left\| (m_w^{\exp})_j - (m_w^{\text{num}})_j \right\| \mathrm{d}t \tag{34}$$

Then, parts of the highly scored solutions are selected to be the parents. Mutation and crossover functions are used on the parents to produce the next generation within the boundary constraints (Eq. (35)).

$$X^L \le X \le X^U \tag{35}$$

where X is the vector of parameters, X^L and X^U are, respectively, the lower and the upper bounds given in Table 3. Finally, the minimization is terminated either when the error is lower than a tolerance limit or when the maximum number of generations is reached.

Table 2
Settings used in the optimization process with the MATLAB genetic algorithm.

Option	Setup value
Population size	50
Generations number	100
Initial population range	[0 1]
Crossover function	@crossoverscattered
Crossover fraction	0.5
Mutation function	@mutationadaptfeasible
Tolerance in fitness value	1×10^{-7}

We used the GA ToolBox in the MATLAB Software with the options listed in Table 2. The model reproduced all the experimental results (%RH, thickness) with the identified parameters given in Table 3. The simulated mass uptake (Eq. (33)) is compared with the gravimetric results in Figs. 7(a), (b) and 8, respectively for the experiments performed under 40%RH, 60%RH and 90%RH. The respective contributions of w and Y are plotted in the figures Fig. 8(a), (b) and (c), for the samples aged at 90%RH.

6. Discussion

6.1. Reaction process

The rate law formulation initially suggested by [15] was supported by (1) experimental observations showing that polymers that contain residual epoxy groups display a two-stage sorption behavior and by (2) the possible reaction between the epoxy group and the water forming a diol. In the present work, we should reconsider the nature of the reactive sites involved in the hydrolysis, as the resin is cured with an anhydride whereas [15] investigated amine/epoxy system. An anhydride cross-linked polymer presents several chemical groups that can be hydrolyzed:

- The residual epoxy groups that are either in excess with respect to the hardener or remain because of the incomplete curing.
- The residual anhydride groups that are likewise in excess if the ratio of epoxy/hardener is not stoichiometric or if the cross-linking is not completed. These groups are hydrolyzed faster than the epoxy groups.
- The ester groups formed by the epoxy—anhydride reaction. It is worth noting that the ester hydrolysis is slower than that of the epoxy.

According to the material description, the ratio epoxy/anhydride is equal to 1, the three aforementioned groups are therefore present.

The formulation proposed by Tcharkhtchi et al. [15] does not account for the reverse reaction, suggesting that the mass of water retained in the polymer in the form of a diol was not desorbed and leading to a constant residual mass. The desorption tests performed here clearly show that the reverse reaction has, on the contrary, to be taken into account. Hence, during desorption, the dissociation of Y, which occurs at a slower rate than its formation, releases the water molecules that are then removed from the polymer. The kinetics proposed by [26] and adopted here is therefore more suitable. This point highlights the relevance of the desorption test to a full understanding of sorption kinetics. Nevertheless, more investigations need to be conducted to clearly identify desorption mechanisms. Previous studies [28,29] reported that residual water, after an absorption test, is removed more quickly with increasing temperature. The experimental results presented here show that the residual concentration of water in the polymer increases with increasing relative humidity.

Table 3
Parameters of the diffusion-reaction model: optimal values identified from the gravimetric experiments and bounds used in the optimization process.

Parameter	Unit	Optimal value	Lower bound	Upper bound
D_0	$m^2\ s^{-1}$	5×10^{-12}	3×10^{-12}	7×10^{-12}
S_0	$mol\ m^{-3}\ Pa^{-1}$	0.0635	0.0375	0.1
D_1	$m^5\ mol^{-1}\ s^{-1}$	-1.24×10^{-14}	-7.75×10^{-14}	7.75×10^{-14}
S_1	Pa^{-1}	1.676×10^{-4}	0.5×10^{-4}	4×10^{-4}
R_0	$mol\ m^{-3}$	3.87×10^{3}	0.3×10^{3}	6.5×10^{3}
k_h	$m^3\ mol^{-1}\ s^{-1}$	8.535×10^{-10}	0.775×10^{-10}	77.5×10^{-10}
k_r/k_h	$mol\ m^{-3}$	6.5×10^{3}	0.4×10^{3}	16×10^{3}

Despite differences in the physical interpretations, it is worth noting the formal analogy between the retained rate law (Eq. (21)) and the classical Carter and Kibler model [23,24]. In the latter, the time evolution of Y (Eq. (36)) is deduced from a probabilistic approach where the parameters γ and β (s^{-1}) are, respectively, the probabilities of release and capture of a water molecule.

$$r_w^{CK} = -\frac{\partial Y}{\partial t} = \beta Y - \gamma w \tag{36}$$

Considering that the diffusion behavior is linear (constant D and S), as assumed in Carter and Kibler's original model, the optimization process did not lead to a satisfying solution, even for a single experimental condition (%RH, thickness). This was confirmed by a parametric analysis performed on β and γ. It is worth noting that, for a given experimental test, the model can reproduce the absorption test with a set of parameters (γ, β), but it cannot simultaneously fit the absorption and desorption curves. The absolute value of the discrepancy between Carter and Kibler's model and the results of the experimental test conducted at 60%RH (435 μm) is more than 10 times higher than it is for the proposed model. The assumptions of Carter and Kibler's model need to be reconsidered in the present case. Using the non constant diffusivity (D_0, D_1) and solubility (S_0, S_1) identified in the previous section and the parameters (γ, β) according to the Eq. (37) (analogy between Eq. (21) and Eq. (36)), numerical simulations give results equivalent to the model proposed in this work.

$$\beta = k_r \quad \gamma = k_h R_0 \tag{37}$$

The reason for this is that the variations of R are negligible (less than 5% in relative values) and the approximation $R = R_0$ is reasonable in the present case.

Another approach is proposed by [17] to model the two-stage sorption behavior of a toughened commercial epoxy. After an absorption-desorption test, they reported that the mass uptake was reversible, meaning that almost all the water was desorbed, whereas a remaining volumetric expansion was observed. SEM observations confirmed the creation of micropores within the polymer. This microstructural modification could in part explain the non-Fickian behavior. In Ref. [17], authors adopted a phenomenological approach with a set of user-defined functions, for the non-linear diffusion behavior and the reaction term, that agreed well with the experimental curves. As their results differ in some points from the observations presented here, it is interesting to see how the present model can be extended. First, Eq. (29) should include another term to specify the fact that sites can be created during the absorption process, unlike the case we considered here where we assume that R is initially imposed and that its evolution is the result of consumption by the reaction (Eq. (38)). The function $f(T,w)$ would correspond to the description of the cavitation process ($f > 0$) if R refers to the micropores. On the other hand, if we consider R as the epoxy or the anhydride groups (hydrolysis model)

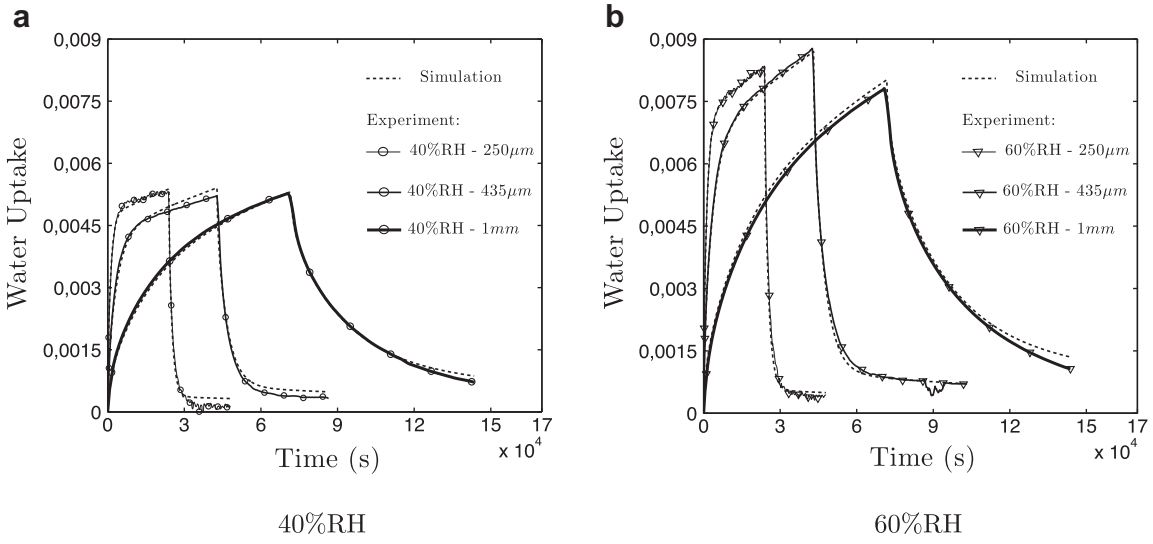

Fig. 7. Evolution of the simulated mass uptake (Eq. (33)) compared to the gravimetric experiments performed under 40% and 60%.

$f(T,w)$ could describe the eventual curing ($f < 0$) of the polymer (for stoichiometric mixtures) with longer exposure time.

$$\frac{\partial R}{\partial t} = -k_h w R + k_r Y + f(T,w) \tag{38}$$

Finally, it should be noted that in the case of different mechanisms involved, the reaction can be expected to be at a higher order than 1. In this case, the reaction kinetics should be modified (Eqs. (28), (29) and (30)).

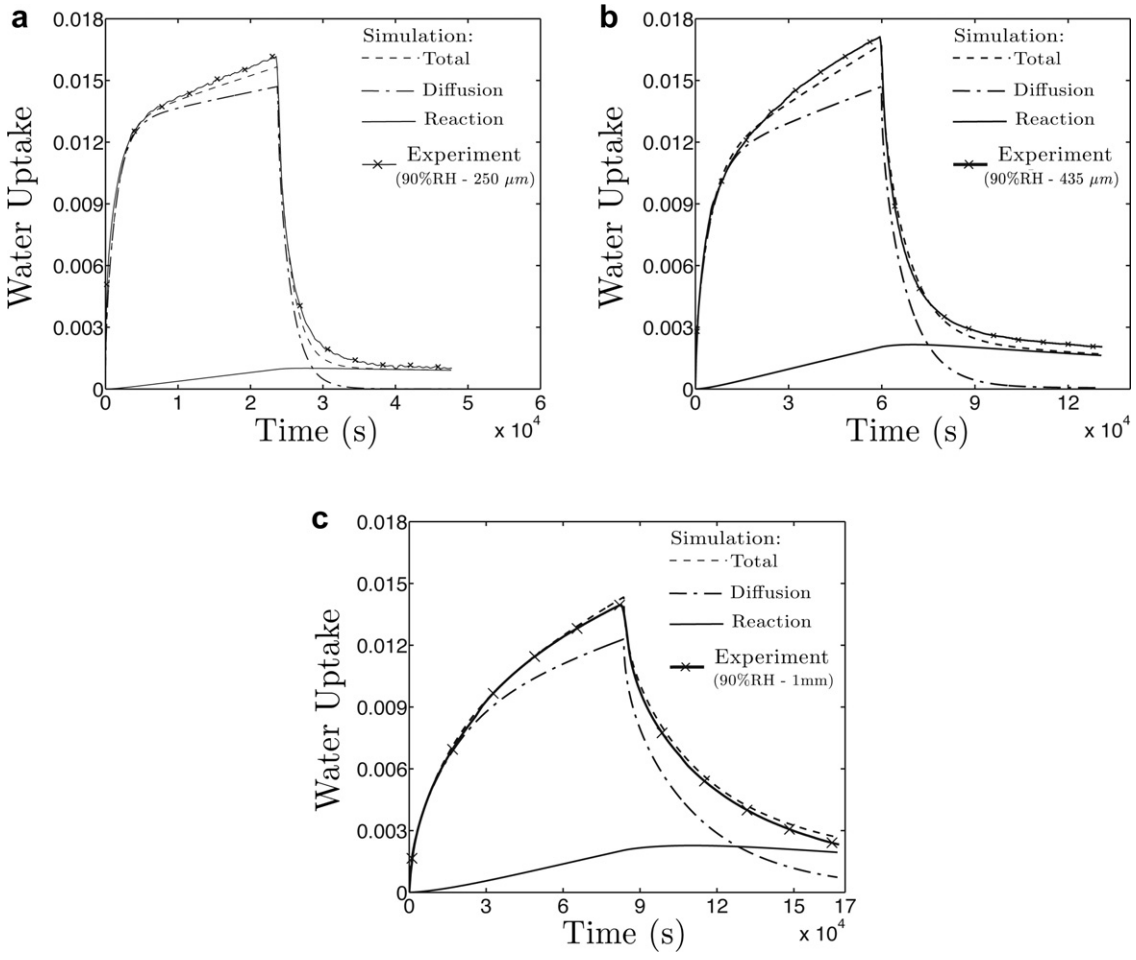

Fig. 8. Evolution of the simulated mass uptake (Eq. (33)) and the respective contributions of diffusion (w) and reaction (Y): Comparison to the gravimetric experiments performed under 90% RH.

6.2. Non-linear diffusion

As mentioned above, Carter and Kibler's model fails to reproduce both the absorption and desorption tests. The main reason is the assumption of linear diffusion behavior. In the present work, we consider that both the diffusion parameter and the solubility are affected by the transformation due to the reaction.

6.2.1. Solubility increase

The solubility of the polymer increases ($S_1 > 0$) with the advancement of the reaction (Eq. (27)). The evolution of the average solubility during the absorption–desorption test, for the 1 mm thick sample, is plotted in Fig. 9.

For the purpose of physical interpretation, we introduce the dimensionless number, N_Y, defined according to Eq. (39). From a global point of view, N_Y is the molar contribution of the complex Y to the polymer hydrophilicity. In other words, for 1 mol of Y created by the reaction (Eq. (20)), N_Y is the number of moles of water fixed by the polymer. For the system under study, the average value of N_Y is estimated to be 0.8, 1.19 and 1.78 for water activity in the environment (a^e) equal to 0.4, 0.6 and 0.9, respectively.

$$N_Y = S_1 \cdot a^e \cdot p_{sat} \tag{39}$$

A physical interpretation can be provided if we consider that hydrolysis of anhydride, epoxy or ester, forms two hydrophilic sites (2 acids for the anhydride, 2 alcohols for the epoxy and 1 acid with 1 alcohol for the ester). Hence, the molar contribution of the hydrophilic group is equal to $N_{OH} = N_Y/2$ and takes the values of 0.4, 0.6 and 0.89, respectively, for water activity in the environment (a^e) equal to 0.4, 0.6 and 0.9. This result is consistent with the observations in the literature that report values lower than unity [30], suggesting that only a fraction of the created hydrophilic sites is able to fix a water molecule and participate in the solubility increase.

6.2.2. Diffusivity decrease

On the contrary, the diffusion parameter decreases ($D_1 < 0$) with the advancement of the reaction (Eq. (26)). The evolution of the average diffusivity during an absorption–desorption test, for a 1 mm thick sample, is plotted in Fig. 10.

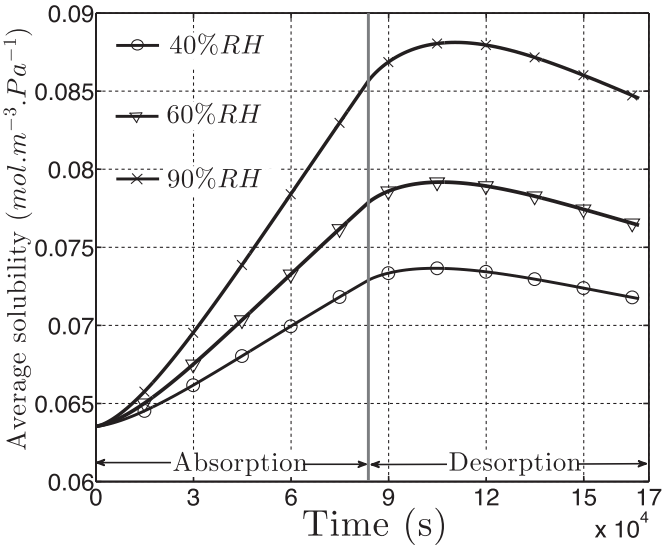

Fig. 9. Evolution of the average solubility as the reaction advances during absorption and desorption.

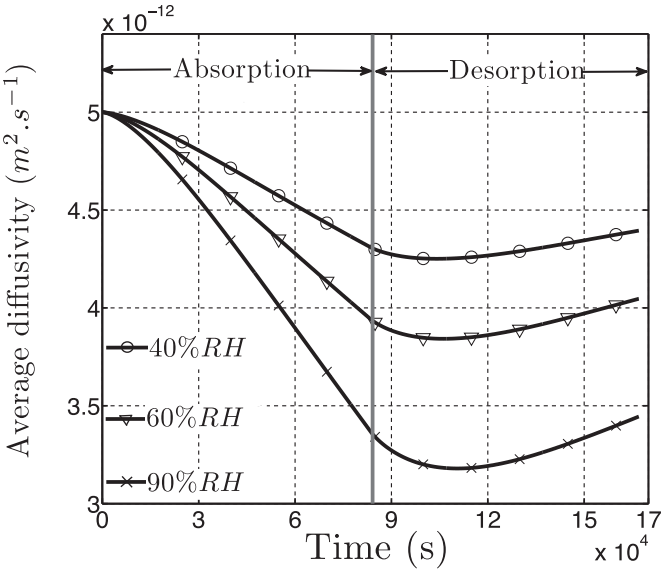

Fig. 10. Evolution of the average diffusion parameter as the reaction advances during absorption and desorption.

By combining Eqs. (26) and (27), we obtain the following linear relation between the local diffusion parameter (D) and the local solubility (S) (Eq. (40)):

$$D - D_0 = \delta(S - S_0) \tag{40}$$

where δ (m^5 Pa mol^{-1} s^{-1}) is defined as the ratio D_1/S_1.

This dependency has been previously highlighted by Belenger et al. [31] for amine-epoxy systems and by [32] for different polymers. The relationship between solubility and diffusivity, as identified in this work, is compared in Fig. 11 to the experimental results obtained by [31]. In the three epoxy systems, the diffusivity decreases linearly as a function of the solubility. The slope δ is equal

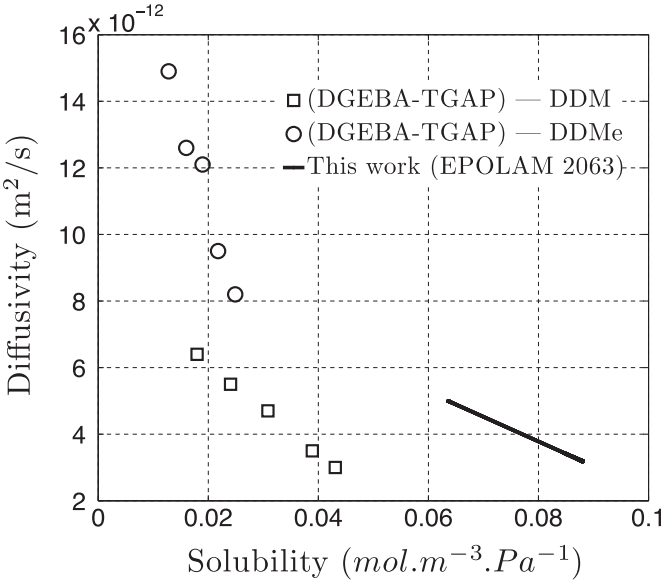

Fig. 11. Relationship between solubility and diffusivity (1) as identified in this work ($\delta = -0.74 \times 10^{-10}$) (2) for the DGEBA-TGAP/DDM epoxy system [31] ($\delta = -1.35 \times 10^{-10}$ with $\rho = 1200$ kg m) (3) for the DGEBA-TGAP/DDMe epoxy system [31] ($\delta = -5.5 \times 10^{-10}$ with $\rho = 1200$ kg m).

Table 4
Comparison of the reaction characteristic time ($\kappa = 1/(k_h \cdot R_0)$) and the diffusion characteristic time ($\tau_D = L^2/D_0$).

Thickness (mm)	τ_D (10^4 s)	κ/τ_D
0.25	1.25	24.2
0.435	3.78	8
1	20	1.5

to -0.74×10^{-10} in the present work, to be compared to the values reported for the two epoxy-amine systems (in which density is approximated by 1200 kg m^{-3}): (1) $\delta = -1.35 \times 10^{-10}$ for DGEBA-TGAP/DDM (2) $\delta = -5.5 \times 10^{-10}$ for DGEBA-TGAP/DDMe. Consequently, as a first conclusion, the identified values for D_1 and S_1 as well as the associated trend are consistent with the data available in the literature.

In order to explain this experimental observation, Merdas et al. [30] considered the diffusion of water as a sequence of three steps.

(1) A molecule of water that is bonded to a hydrophilic site, P_1, is released by breaking the low energy bond.
(2) The water molecule migrates from the site, P_1, to another site, P_2.
(3) The molecule is captured by forming a hydrogen bond with the site, P_2.

If either steps (1) or (3) is the limiting process, the apparent diffusivity will decrease if the distance between the two hydrophilic sites decreases. Yet, this distance is a decreasing function of the hydrophilic group density.

Finally, the solubility increase and the diffusivity-solubility relationship both demonstrate the hydrophilicity of the product of the reaction Y.

6.3. Concentration gradients

In this section, we discuss the spatial distribution of the concentrations of the diffusing particles (w) and the product of the reaction (Y). The competition between the diffusion and the reaction can obviously affect the concentration profiles of the two species and consequently the stress/strain distribution and the local mechanical properties. Two different time scales are relevant to describe the evolution of these profiles: $\tau_D = L^2/D_0$ is the diffusion characteristic time and $\kappa = 1/(k_h \cdot R_0)$ is the reaction characteristic time (Table 4).

In Figs. 12 and 13, the local concentrations of w and Y are respectively plotted in the reduced coordinates (normalized by $w_{S0} = S_0 \cdot a^e \cdot p_{sat}$ for w and Y and by the half thickness for the position) and at several reduced times, $t_D^* = t/\tau_D$ and $t_R^* = t/\kappa$.

Fig. 12 shows that for times such as $t_D^* \leq 0.6$, all the profiles of w are superimposed, which is characteristic of a Fickian equation ($\forall\ t$). The concentration gradients of w are attributed to the diffusion process. With longer exposure times, the concentration profiles of w are either almost homogeneous (for thin samples) or they exhibit gradients (for thick samples and high %RH) that are in this case attributed to the reaction process. Indeed, Fig. 13 shows

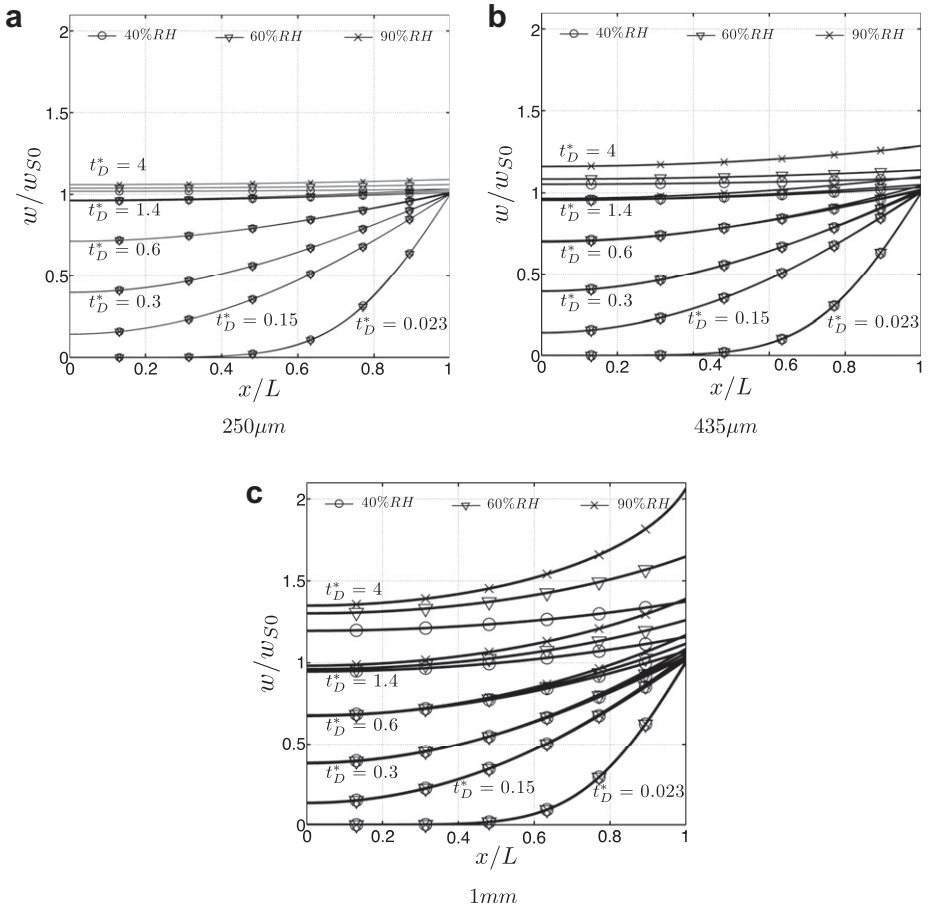

Fig. 12. Concentration profiles of w plotted in the reduced coordinates (normalized by $w_{S0} = S_0 \cdot a^e \cdot p_{sat}$ for w and by the half thickness for the position x) and at several reduced times $t_D^* = t/\tau_D$.

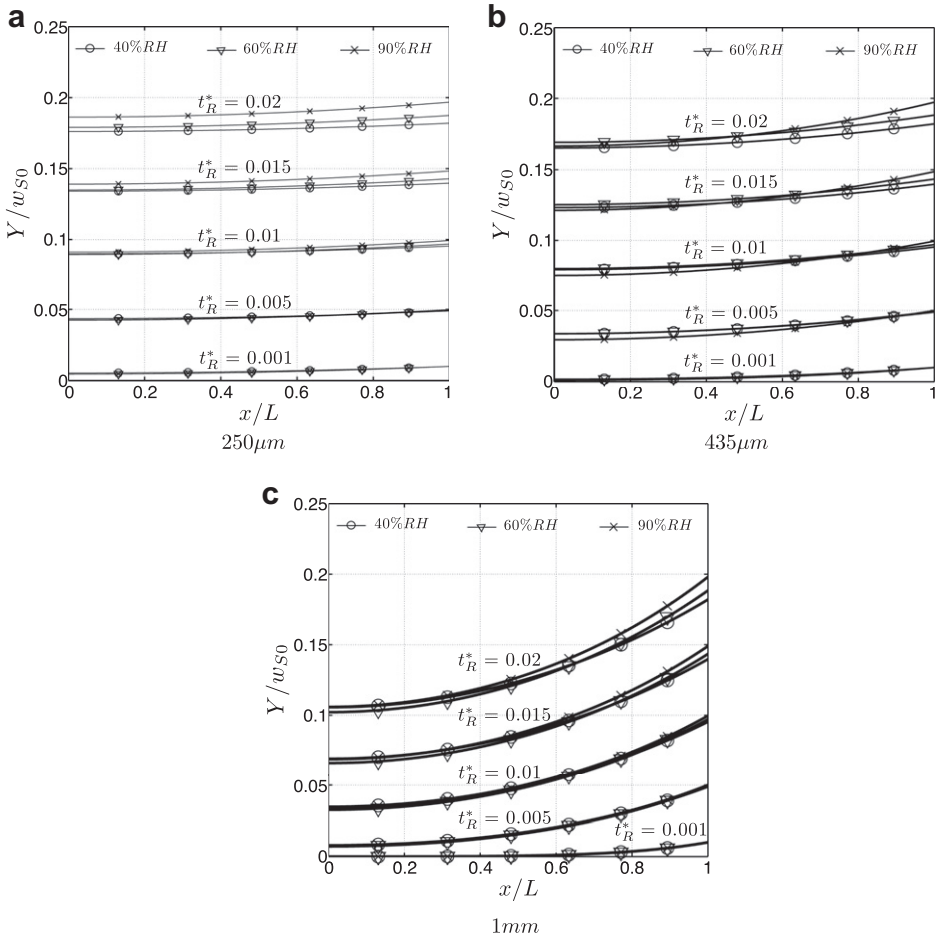

Fig. 13. Concentration profiles of Y plotted in the reduced coordinates (normalized by $w_{S0} = S_0 \cdot a^e \cdot p_{sat}$ for Y and by the half thickness for the position x) and at several reduced times $t_R^* = t/\kappa$.

that the concentration of the product Y along the thickness is almost homogeneous in the thin samples (Fig. 13(a), (b)), whereas gradients are observed in the thicker sample (Fig. 13(c)).

Under static conditions (i.e., constant temperature and constant %RH), the ratio of characteristic times (τ_D, κ) traduces the competition between the diffusion and the reaction, and the two following situations are representatives of the experimental cases (Table 4):

$\tau_D \ll \kappa$: After reaching the pseudo-saturation level ($t \simeq 2\tau_D$), the profile of concentration w evolves with the reaction but can be considered as homogeneous throughout the thickness. In this case, the diffusion and the reaction processes are well dissociated.

$\tau_D \simeq \kappa$: For high %RH, we can expect strong gradients even after the pseudo-saturation. It is worth noting that a linear diffusion behavior (Fickian model or Carter and Kibler's model) would lead to homogeneous field of w. This coupling between diffusion and reaction will significantly affect the local stress/strain.

To complete this discussion, we should consider cyclic conditions by taking into account the associated period T_C. Currently, we are investigating the effect of cyclic conditions. We expect a significant effect of the ratios of the characteristic times, (τ_D, κ, T_C), on the resulting concentration profiles and local hygrothermoelastic stress ([33,34]). The cycling conditions that lead to strong concentration gradients will potentially result in material damage.

7. Conclusion

- In this work, we demonstrated that absorption−desorption tests are relevant to capture non-classical sorption behaviors of epoxy polymers. In particular, we confirm the reversibility of the non-Fickian mechanisms (second-stage). Also, we show that Carter and Kibler's model is not appropriate in the present case, although it would have been possible to use it to reproduce the absorption test separately.
- The scheme proposed in this paper describes water transport as a competition between (1) diffusion, which can involve several fundamental mechanisms (free volume, water/polymer interaction), and (2) a reactive process that can induce a certain evolution of the polymer (structure or microstructure). In addition to diffusive transport, some physical phenomena are potentially responsible for trapping water molecules and modification of the diffusive behavior.
- We showed that the non-linear diffusion behavior is due to the hydrophilicity of the product of the reaction (Y). The augmentation of the hydrophilic sites density explain the solubility increase and the diffusivity decrease.
- Incomplete curing of the polymer can justify part of the phenomenology because of the presence of hydrolyzable groups (anhydride, epoxy).
- The evolution of the local material properties that comes with the reaction can strongly modify the water concentration field.

The resulting gradients should be carefully examined for durability assessment.

References

[1] McKague E, Reynolds J, Halkias J. Swelling and glass transition relations for epoxy matrix material in humid environments. J Appl Polym Sci 1978;22: 1643–54.
[2] De Neve B, Shanahan M. Water absorption by an epoxy resin and its effect on the mechanical properties and infra-red spectra. Polymer 1993;34:5099–105.
[3] Zhou J, Lucas J. Hygrothermal effects of epoxy resin. part ii: variations of glass transition temperature. Polymer 1999;40:5513–22.
[4] Perrin F, Nguyen M, Vernet J. Water transport in epoxy-aliphatic amine networks - influence of curing cycles. Eur Polym J 2009;45:1524–34.
[5] Alessi S, Conduruta D, Pitarresi G, Dispenza C, Spadaro G. Accelerated ageing due to moisture absorption of thermally cured epoxy resin/polyethersulphone blends. thermal, mechanical and morphological behavior. Polym Degrad Stab 2011;96:642–8.
[6] Adamson M. Thermal expansion and swelling of cured epoxy resin used in graphite/epoxy composite materials. J Mater Sci 1980;15:1736–45.
[7] Wong T, Broutman L. Moisture diffusion in epoxy resins part 2. diffusion mechanism. Polym Eng Sci 1985;25(9):529–34.
[8] Xiao G, Shanahan M. Swelling of dgeba/dda epoxy resin during hygrothermal ageing. Polymer 1998;39(14):3253–60.
[9] Vanlandingham M, Eduljee R, Gillespie J. Moisture diffusion in epoxy systems. J Appl Polym Sci 1999;71:787–98.
[10] Karalekas D, Cugnoni J, Botsis J. Monitoring of hygrothermal ageing effects in an epoxy resin using fbg sensor: a methodological study. Comp Sci Technol 2009;69:507–14.
[11] Crank J. The mathematics of diffusion. 2nd ed.; 1975.
[12] Illinger J, Schneider N. Water vapor transport in an epoxy resin based on tgmda and dicy. Polym Eng Sci 1980;20(4):310–4.
[13] Wong T, Broutman L. Moisture diffusion in epoxy resins part 1. non-fickian sorption processes. Polym Eng Sci 1985;25(9):521–8.
[14] Johncock P, Tudgey G. Some effects of structure, composition and cure on the water absorption and glass transition temperature of amine-cured epoxies. Br Polym J 1986;18(5).
[15] Tcharkhtchi A, Bronnec P, Verdu J. Water absorption characteristics of diglycidylether of butane diol-3,5-diethyl-2,4-diaminotoluene networks. Polymer 2000;41:5777–85.
[16] Al-Harthy M, Loughlin K, Kahraman R. Moisture diffusion into epoxy adhesive: testing and modeling. Adsorption 2007;13:115–20.
[17] Leger R, Roy A, Grandidier J. Non-classical water diffusion in an industrial adhesive. Int J Adhes Adhes 2010;30:744–53.
[18] Placette M, Fan X. A dual stage model of anomalous moisture diffusion and desorption in epoxy mold compounds. In: 12th Int. Conf. on thermal, mechanical and multiphysics simulation and experiments in microelectronics and microsystems; 2011.
[19] Bhattacharyya B, Huffman W, W.E. J, Natarajan B. Moisture absorption and mechanical performance of surface mountable plastic packages. In: Electronic components and technology conference; 1988. p. 49–58.
[20] Wong E, Chan K, Lim T, Lam T. Non-fickian moisture properties characterisation and diffusion modeling for electronic packages. In: Electronic components and technology conference; 1999. p. 302–6.
[21] Lin Y, Chen X. Moisture sorption-desorption-resorption characteristics and its effect on the mechanical behavior of the epoxy system. Polymer 2005;46: 11994–2003.
[22] Weitsman Y. A continuum diffusion model for viscoelastic materials. J Phys Chem 1990;94:961–8.
[23] Carter H, Kibler K. Langmuir-type model for anomalous moisture diffusion in composite resins. J Composite Mater 1978;12:118–31.
[24] Popineau S, Rondeau-Mouro C, Sulpice-Gaillet C, Shanahan M. Free-bound water absorption in an epoxy adhesive. Polymer 2005;46:10733–40.
[25] Gautieri A, Vesentini S, Redaelli A. How to predict diffusion of medium-sized molecules in polymer matrices. from atomistic to coarse grain simulations. J Mol Model 2010;16:1845–51.
[26] Didierjean S. Etude du comportement des materiaux composites carbone/epoxy en environnement hygrothermique. Ph.D. thesis; 2004.
[27] Vanlandingham M, Eduljee R, Gillespie J. Relationships between stoichiometry, microstructure, and properties for amine-cured epoxies. J Appl Polym Sci 1999b;71:699–712.
[28] Zhou J, Lucas J. Hygrothermal effects of epoxy resin. part i: the nature of water in epoxy. Polymer 1999b;40:5505–12.
[29] Lin Y. Investigation of the moisture-desorption characteristics of epoxy resin. J Polym Res 2006;13:369–74.
[30] Merdas I, Thominette F, Tcharkhtchi A, Verdu J. Factors governing water absorption by composite matrices. Comp Sci Technol 2002;62:487–92.
[31] Bellenger V, Verdu J, Morel E. Structure-properties relationships for densely cross-linked epoxide-amine systems based on epoxide or amine mixtures: part 2: water absorption and diffusion. J Mater Sci 1989;24:63–8.
[32] Thominette F, Gaudichet-Maurin E, Verdu J. Effect of structure on water diffusion in hydrophilic polymers. Defect Diff Forum 2006;258–260: 442–6.
[33] Gigliotti M, Jacquemin F, Vautrin A. Assessment of approximate models to evaluate transient and cyclical hygrothermoelastic stress in composite plates. Int J Solids Struct 2007;44:733–59.
[34] Gigliotti M, Jacquemin F, Molinard J, Vautrin A. Transient and cyclical hygrothermoelastic stress in composite plates: modelling and experimental assessment. Mech Mater 2007;39:729–45.